Linköping Studies in Science and Technology, Thesis No. 1824
Licentiate Thesis

High-Temperature Fatigue Behaviour of Austenitic Stainless Steel

-Influence of Ageing on Thermomechanical Fatigue and Creep-Fatigue Interaction

Hugo Wärner

Division of Engineering Materials
Department of Management and Engineering
Linköping University, SE-581 83, Linköping, Sweden
http://www.liu.se

Linköping, November 2018

Opponent: Professor Johan Ahlström, Chalmers University, Göteborg, Sweden.
Examiner: Associate professor Stefan Lindström, Linköping University, Linköping, Sweden.
Date: 10:15, December 14, 2018
Room: ACAS, Linköping University

Cover:
Filtered image of a thermomechanical fatigue test, highlighting the coil and specimen.

Printed by:
LiU-Tryck, Linköping, Sweden, 2013
ISBN 978-91-7685-174-6

Distributed by:
Linköping University
Department of Management and Engineering
SE-581 83, Linköping, Sweden

This document was prepared with LaTeX, November 12, 2018

Abstract

The global energy consumption is increasing and together with global warming from greenhouse gas emission, create the need for more environmental friendly energy production processes. Higher efficiency of biomass power plants can be achieved by increasing temperature and pressure in the boiler section and this would increase the generation of electricity along with the reduction in emission of greenhouse gases e.g. CO_2. The power generation must also be flexible to be able to follow the demands of the energy market, this results in a need for cyclic operating conditions with alternating output and multiple start-ups and shut-downs.

Because of the demands of flexibility, higher temperature and higher pressure in the boiler section of future biomass power plants, the demands on improved mechanical properties of the materials of these components are also increased. Properties like creep strength, thermomechanical fatigue resistance and high temperature corrosion resistance are critical for materials used in the next generation biomass power plants. Austenitic stainless steels are known to possess such good high temperature properties and are relatively cheap compared to the nickel-base alloys, which are already operating at high temperature cyclic conditions in other applications. The behaviour of austenitic stainless steels during these widened operating conditions are not yet fully understood.

The aim of this licentiate thesis is to increase the knowledge of the mechanical behaviour at high temperature cyclic conditions for austenitic stainless steels. This is done by the use of thermomechanical fatigue- and creep-fatigue testing at elevated temperatures. For safety reasons, the effect of prolonged service degradation is investigated by pre-ageing before mechanical testing. Microscopy is used to investigate the microstructural development and resulting damage behaviour of the austenitic stainless steels after testing. The results show that creep-fatigue interaction damage, creep damage and oxidation assisted cracking are present at high temperature cyclic conditions. In addition, simulated service degradation resulted in a detrimental embrittling effect due to the deterioration by the microstructural evolution.

Acknowledgement

This research has been financially supported by AB Sandvik Materials Technology in Sandviken, Sweden, Sandvik Heating Technology AB in Hallstahammar, Sweden and the Swedish Energy Agency through the Research Consortium of Materials Technology for Thermal Energy Processes, Grant No. KME-701, for which they are all greatly acknowledged. Many thanks to my supervisors Mattias Calmunger, Johan Moverare, Guocai Chai and Sten Johansson for their expertise, guidance and support. Mattias Calmunger deserves even more thanks for the time and encouragement he has given me during this project. I would also like to thank all my colleagues at the division of Engineering Materials for fruitful discussions and creating an enjoyable working environment. The technical support from Patrik Härnman, Annethe Billenius and Rodger Romero Ramirez is also greatly acknowledged.

Finally, I would like to thank my parents, Claes and Ann, for always supporting and believing in me throughout my endeavours.

Hugo Wärner
Linköping, November 2018

List of Papers

In this thesis, the following papers have been included:

I. H. Wärner, M. Calmunger, G. Chai, S. Johansson and J. Moverare, *Creep-fatigue interaction in heat resistant austenitic alloys*, Published online May 25, MATEC Web of Conferences volume 165 (2018).

II. H. Wärner, M. Calmunger, G. Chai, J. Polák, R. Petráš, M. Heczko, T. Kruml, S. Johansson and J. Moverare, *Fracture and Damage Behavior in an Advanced Heat Resistant Austenitic Stainless Steel During LCF, TMF and CF*, presented at ECF22, Belgrad (Serbia), 2018, To appear in Procedia Structural Integrity, ECF22 Proceedings (journal by Elsevier).

III. H. Wärner, M. Calmunger, G. Chai, S. Johansson and J. Moverare, *Thermomechanical fatigue behaviour of aged heat resistant austenitic alloys*, Manuscript, 2018, To be submitted to International Journal of Fatigue.

Contribution to the papers included:

In all papers above, I have been the main contributor of the microstructure investigation, evaluation and manuscript writing. In addition, I have performed the pre-aged thermomechnical fatigue tests, creep-fatigue tests, hardness tests, creep tests and Thermo-Calc simulations. Long term creep data and long term aged specimens has been been provided by AB Sandvik Materials Technology in Sandviken, Sweden.

Contents

Abbreviation

BCC	body-centred cubic
BCT	body-centred tetragonal
BSE	backscattered electron
CF	creep-fatigue
EBSD	electron backscatter diffraction
ECCI	electron channeling contrast imaging
EDS	energy-dispersive spectroscopy
FCC	face-centred cubic
FEG	field emission gun
GB	grain boundary
GBS	grain boundary sliding
IP	in-phase
IPF	inverse pole figure
LCF	low cycle fatigue
MAD	mean angular deviation
OP	out-of-phase
RT	room temperature
SEM	scanning electron microscopy
SE	secondary electron
TMF	thermomechanical fatigue

Part I

Background and Theory

1

Introduction

1.1 Introduction to the research project

This licentiate thesis is a part of KME-701, *Influence of high-temperature environments on the mechanical behaviours of high-temperature austenitic stainless steels*, which is a research project in collaboration between Linköping University, AB Sandvik Materials Technology and Sandvik Heating Technology AB. The research project is partly financed by the Swedish Energy Agency and by industries, through the research consortium of materials technology for thermal energy processes (KME).

1.2 Background

With rising energy consumption the need for renewable energy is great in order to avoid excessive emission of greenhouse gases (e.g. CO_2) [1, 2]. Biomass fuel is one alternative that is renewable in the sense that the amount CO_2 consumed during growth is released during combustion [3]. In the future a need for flexible generation of power is critical if only renewable power generation is to be achieved. The power plants must therefore be able to alter their output, have access to back up power plants or even shutdown during certain periods to be able to follow the demands of the energy market [4, 5]. Also, higher efficiency in power plants is desirable and this can be achieved by increasing pressure and temperature in the boiler sections [6, 7]. This results in not fully investigated operating conditions which may negativley affect the materials in the power plants. These conditions includes alternating- and long term high-temperature, cyclic loading and corrosive environments and they are of great interest if the goals for future power generation are to

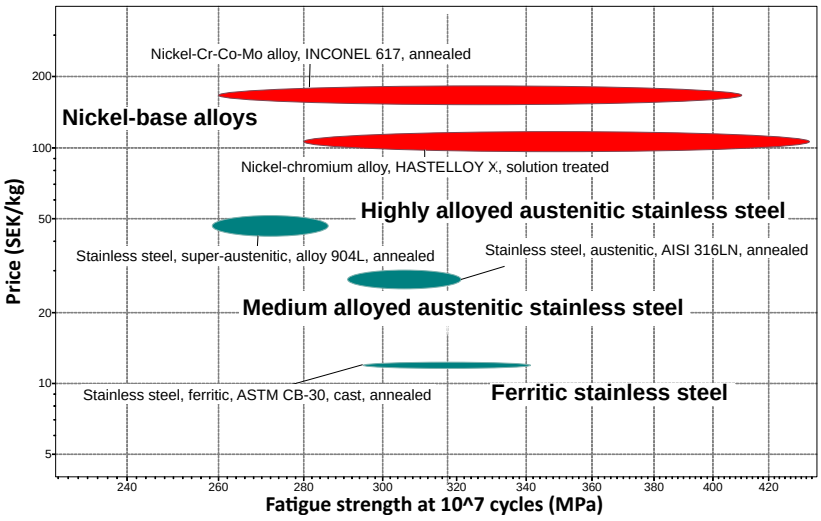

Figure 1: Difference in price [SEK/kg] vs. fatigue strength (max stress to survive 10^7 cycles, RT , R=-1), for power plant materials (From CES EduPack 2018).

be achieved. During start-up and shut-down, the thermal transient and mechanical strain cycles induce strain-temperature phasing, which is known as thermomechanical fatigue (TMF) [8, 9]. In addition, creep reduces the ductility at high temperature, thus accelerating the fatigue damage [10]. This damaging effect is known as creep-fatigue (CF) interaction and together with TMF, they are key damaging factors during these new operation conditions [8, 10].

Traditionally, ferritic stainless steels have been used for power plant materials, but with highly corrosive environments and the demands of increased efficiency other material groups must be considered. There are biomass power plants in which medium alloyed stainless steel are used for components such as boilers, digesters, pumps and valves [11]. Another possible candidate could be the nickel-base alloys, which are already operating in these new conditions in other applications. However, they are expensive compared to austenitic stainless steels and this is shown in Fig. 1. Highly alloyed austenitic stainless steels have comparable resistance to aggressive and high temperature environments as the nickel-base alloys and superior resistance compared to the ferritic stainless steels. This makes them a suitable candidate for the next generation biomass power plants, but the behaviour at these new operating conditions are not fully understood [6, 11].

1.3 Purpose of the research

The KME-701 project specifically addresses the following purpose of the KME-program: "To evaluate the mechanical properties and service life of various materials in relation to new material requirements for more efficient electricity production (elevated pressures and temperatures)" and "To develop methods for quantifying processability for new materials, as well as creating an understanding of microstructure development and mechanical properties for more efficient energy plants". This comprises the main purpose of the research in this licentiate, which is to evaluate the mechanical behaviours of materials in power plants that suffers from tougher environment due to the increasing efficiency demands and cyclic operations. The results are thought to be used for material design and improvement, in order to improve boiler design and for safety considerations.

1.4 Research questions

The research in this licentiate aims to investigate the mechanical behaviour at high temperature cyclic conditions for austenitic alloys, which could be suitable candidates for critical components in the next generation power plants. For safety reasons, the effect of prolonged service degradation is also investigated in order to analyse the durability of the materials. The following research questions (RQ) are the basis of the investigation.

1. During TMF and CF conditions, what are the high-temperature fatigue response and behaviour of the investigated materials?
2. How will prolonged service simulated by pre-ageing influence the high-temperature behaviour during TMF and CF conditions?
3. Which of the investigated austenitic alloys are best suited for critical components in the next generation power plants, considering their TMF and CF performance? Why is this?

1.5 Overview of the thesis

This thesis is divided into two parts. Part I provides background and theory to the research area and consists of six chapters. After an introduction to the research project in Chapter 1, a general presentation of austenitic stainless steel and the effect of alloying elements with precipitation characteristics are given in Chapter 2. Chapter 3 consists of a description of TMF and CF

interaction, together with their influence on austinetic stainless steels. Mechanical testing procedure for TMF and CF, the investigated materials and the used microscopic techniques are then described in Chapter 4. In Chapter 5, a short summary and discussion of the included papers are provided. This is followed by the overall conclusions of the thesis, in Chapter 6, which also includes suggestions for future work. In Part II, the main research of the thesis is described by the three included papers.

2

Austenitic alloys

2.1 Austenitic stainless steels

Iron (Fe)-based alloys with at least 10.5 wt.% chromium (and maximum 1.2 wt.% carbon) are considered stainless steels [12]. The high chromium content leads to formation of a thin dense chromium oxide (Cr_2O_3) film at the surface, providing the corrosion resistance. If the protective layer is damaged or removed, regeneration can be achieved if the surface is exposed to an environment that can produce enough oxygen. This process is referred to as self-passivation [12]. Commonly stainless steel is divided into four groups (see the list below) depending on their main phases: austenite, ferrite and martensite. The last group in the list is based on the heat treatment used [12–14].

- Ferritic
- Austenitic
- Martensitic
- Duplex (austenitic-ferritic)
- Precipitation-hardening

The crystal structure of these main phases are face centred cubic (FCC) for austenite, body centred cubic (BCC) for ferrite and body centred tetragonal (BCT) for martensite. However, the focus of this project is on the behaviour of austenitic stainless steels. In general, the austenitic stainless steels includes 16-26 wt.% chromium, 8-25 wt.% nickel, 0-6 wt.% molybdenum and lower

amount of other alloying elements [15]. More about these and their general purposes are covered in the next section. Becausue of the high chromium content, austenitic stainless steels exhibit great corrosion resistance which indcludes high steam oxidation resistance at elevated temperatures. Other properties such as good weldability and creep resistance, excellent formability and ductility are commonly associated with austenitic stainless steels [14–16]. But compared to other stainless steel groups, they also have low diffusivity and high coefficcient of expansion, which can be problematic when used in dissimilar welds. Due to the fact that austenitic stainless steels are not susceptible to hydrogen embrittlement, in most cases there is no need for pre- and post-weld heating [16]. Increase of strength can be achieved by cold working but normally not by heat treatments [15].

2.1.1 Alloying elements

Different main alloying elements of austenitic stainless steels promote different types of microstructures. In order to keep the appropriate microstructure and gain the best properties for a specific application, a balance of the stabilizing elements must be achieved. The alloying additions below are considered in an iron-base material.

Chromium (Cr) is the main alloying element in stainless steel and it provides the alloy with corrosion resistance at high temperatures, as described in the last section. Promotion of the ferritic microstructure is also increased by chromium [15, 17].

Nickel (Ni) promotes the austenitic microstructure and generally increases ductility and toughness and together with chromium it provides the high temperature resistance in austenitic stainless steels [15].

Manganese (Mn) generally improves hot ductility, but it also increases the solubility of nitrogen (N) and promotes the austenitic microstructure. Due to the high cost of nickel, manganese is often used to replace some of the nickel content in certain alloys. [17, 18].

Copper (Cu) promotes the austenitic microstructure and when finley homogenously dispersed, it enhances strength and hardening during high-teperature faigue [19]. It also enhances the formability and machinability [18].

Silicon (Si) promotes the ferritic microstructure and increases the oxidation resistance [15, 18].

Both carbon (C) and nitrogen (N), strongly promote the austenitic microstructure and increase the mechanical strength by solid solution. Carbon reduces resistance of intergranular corrosion due to carbide formation (most often chromium carbides). Titanium (Ti) and niobium (Nb) are added if the

carbon content is relatively high and these two elements reacts more easily with carbon than chromium does, thus lowering the amount of carbide formation in the grain boundaries. In nitrogen containing austenitic stainless steels, niobium also form nitrides which provides strength when finely dispersed [19]. Both niobium and titanium promote the ferritic microstructure [15, 20].

Tungsten (W) generally increase pitting corrosion by stabilization of the oxide layer and also provide solid solution strengthening when finely dispersed throughout the grains [18, 19].

Molybdenum (Mo) is a ferrite stabiliser and improves both the creep properties and the corrosion resistance [20].

2.1.2 Precipitation

At high-temperature conditions, austenitic stainless steels commonly form secondary phases, carbides, nitrites and intermetallic phases [17, 21]. Precipitations like these are often undesirable, because of their detrimental effect on the mechanical properties and corrosion resistance. However, when stable precipitates act as obstacles for dislocation movements they can strengthen alloys. Below, common precipitates in austenitic stainless steels are presented.

$M_{23}C_6$ has a FCC crystal structure and in austenitic stainless steels, the main element (M) is usually chromium. The carbide generally nucleates relatively easy and fast at grain boundaries, twin boundaries and as intragranular precipitates. It commonly depletes chromium in the grain boundaries, leading to intergranular corrosion by sensitisation [17, 22]. For some cases the creep strength are improved, but the fatigue properties are reduced due to an embrittling effect [22].

M_6C has a variable combination of elements for M, these includes chromium, iron, molybdenum, niobium and silicon [17]. It has a FCC structure and generally forms in austenitic stainless steel with enough molybdenum or niobium, after long-term ageing [21]. It can be hard to distinguish M_6C from $M_{23}C_6$ because of resembling formation sites and morphologies [23].

Cr_2N has a hexagonal close packed (HCP) crystal structure. At 900 °C, it is found in non-stabilized high niobium containing austenitic stainless steels. In both low nitrogen non-stabilised creep resistant austenitic stainless steels and in stabilised nitrogen grades, Cr_2N is not commonly found. In the latter case it is because Z phase forms instead [17]

MX (MC) precipitates forms in austenitic stainless steels containing strong carbide/nitride formers, such as titanium, niobium, vanadium, zirconium,

tantalum (as M) and nitrogen or carbon or both (as X) [17, 24]. The MX precipitates usually form within dislocations or stacking faults and on grain- and twin boundaries. Dispersed MX precipitates increases the creep rupture strength and intergranular corrosion resistance, but they can lower the creep ductility if not the optimum stoichiometry balance is achieved [17, 22].

Z phase has a BCT crystal structure and is a carbonitride that forms in niobium containing, high nitrogen, austenitic stainless steels. The Z phase is usually stable at high-temperature and similar to MX precipitates, it generally forms at grain boundaries, on twin boundaries and within the matrix where dislocations exists [23]. Finely dispersed Z phases, is usually beneficial for the creep resistance, but in some materials the precipitates coarsens with increasing temperature and time and this have the opposite effect on the creep properties [17, 22]. In niobium containing austenitic stainless steels, which has a relatively high level of nitrogen compared to carbon, this effect occurs when Z phase nucleates instead of Nb(C,N) precipitates. Although both Nb(C,N) and the Z phase can be present at the same time in regions of high niobium content [17, 19, 22].

Sigma phase (σ-phase) is an intermetallic phase that consists of iron, chromium, nickel, molybdenum, silicon and it has a tetragonal crystal structure [17]. It often precipitates between 600 °C and 1000 °C and due to its brittle and hard matrix, it increases the hardness of the material. However, it also decreases the toughness, elongation, thermal fatigue and corrosion resistance (by depletion of chromium and molybdenum). If σ-phase forms as large precipitates or as a film in grain boundaries, it is detrimental to the creep resistance. However, if it forms as small intragranular precipitates, it is found to increase the creep resistance [25]. Generally, σ-phase forms at grain and twin boundaries [17, 25]. Nickel and nitrogen usually suppresses formation of σ-phase in austenitic stainless steels [22, 25].

Laves phase is also an intermetallic phase with hexagonal crystal structure and it usually consists of iron, molybdenum, titanium, niobium, silicon, chromium and nickel [26, 27]. In niobium containing steels, Laves phase is detrimental for the creep properties because it promotes formation of M_6C [17]. But in high nickel austenitic stainless steels with tungsten, it is found that the formation of Laves phase in the grain boundaries may improve the creep strength [28]. Generally Laves phase is found dispersed inside the grains, but sometimes also at grain boundaries after long time high-temperature exposure between 600 °C and 1000 °C. In niobium and tungsten containing austenitic stainless steels it can form as Fe_2Nb and/or Fe_2W after ageing around 600 °C and 800 °C [21, 26, 27].

3

Influence of thermomechanical fatigue and creep-fatigue interaction on austenitic stainless steel

This chapter presents the damaging processes acting upon austenitic stainless steels caused by thermomechanical fatigue and creep-fatigue interaction. As mentioned in Chapter 1.2, these two processes significantly lower the fatigue life of critical components in power plants and are considered key factors, along with oxidation, in the understanding of the material behaviour during future operating conditions. Critical power plant components, such as piping in the boiler sections, suffer from stresses and strains originating both from non-uniform temperature fields and internal pressure, which together are found to lower the predicted life of the component [29–31]. Depending of the nature of the future cyclic work in power plants, different type of thermomechanical phasing may occur [8, 29]. In addition, it is well known that the combination of creep and fatigue also exert detrimental effects on components in the boiler sections of power plants and conservative design development is suggested by Code Cases of ASME, for these types of conditions [10, 32–34].

3.1 Thermomechanical fatigue

TMF loading conditions involve thermal transience with mechanical cycling which causes complex evolution of damage. Different types of phasing can arise during this process and the most common ones during testing are the in-phase (IP) and out-of-phase (OP) [8, 9]. Thier respective charactheristics

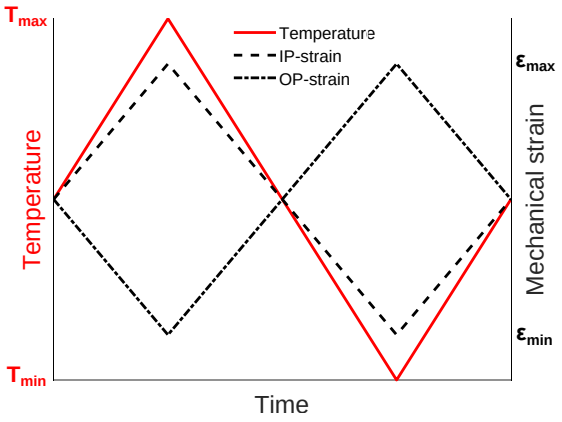

Figure 2: The most common TMF test cycles, in-phase (IP) and out-of-phase (OP).

are shown in Fig. 2. The main damaging contributions are considered to be creep, fatigue and environmental effects (commonly oxidation) [8]. In the work by Nitta and Kuwabara [35], TMF-life behaviour of the two phases are described. Type-I scenario is when IP loading conditions cause earlier failure than OP loading and in this case, creep is the predominant damaging mechanism. This is because of high temperature and tensile stresses, which is more detrimental during IP cycling. In the type-O scenario, OP loading conditions lead to shorter fatigue life due to environmental effects such as embrittlement of the surface which causes early crack initiation. This process effects OP cycling more than IP cycling. If neither environmental effects nor creep damage dominate, IP and OP loading conditions show nearly the same fatigue life. This is the Type-E scenario. In the last scenario, Type-E', IP loading conditions lead to short fatigue life at high strain amplitudes, which means that creep only occurs at high loads [35].

Form the works of H.J. Christ [8], the environmental effect during TMF-conditions for the austenitic stainless steel AISI 304L were investigated. It was found that the alloy had moderate influence from environmental effects and compared to vacuum conditions, interaction with air caused grain boundary oxidation which consequently caused premature crack initiation. This effect was active during OP conditions when creep damage was negligible. Bae et al. [36] also performed investigations of the TMF behaviour for AISI 304L and at higher temperature ranges, 450 °C to 700 °C, creep were found to be the dominant damaging mechanism for IP loading conditions.

TMF test at lower temperature ranges (100 °C to 340 °C) and at higher temperature ranges (300 °C to 650 °C) for the austenitic stainless steels

316L(N), were performed by Mageshwaran et al. [37] and Nagesha et al. [38]. At lower temperature ranges the TMF-life for IP cycling were longer than both OP cycling and isothermal cycling (at T_{max}). However, with increasing TMF peak temperature this difference was found to diminish. At higher temperature ranges, the environmental influence by oxidation on the TMF-life was prominent for OP loading conditions.

Petráš et al. [39] performed investigations on the austenitic stainless steel Sanicro 25, subjected to both IP- and OP loading conditions in the temperature range of 250 °C to 700 °C. Sanicro 25 showed prominent cyclic hardening during these conditions and the most detrimental testing condition was IP loading. This was due to the difference in oxidation assisted crack initiation and growth between IP and OP. For IP tests oxide cracking occured in the grain boundaries, while the OP test showed delayed local oxide cracking in the perpendicular direction. This indicates that creep should be the most damaging mechanism in this case, according to [35].

3.2 Creep-fatigue interaction

The general mechanisms that contribute to creep are commonly classified as dislocation slip, dislocation climb, grain-boundary sliding and diffusion flow caused by vacancies [40, 41]. Both dislocation slip (glide) and dislocation climb are often referred to as dislocation creep, but they have different movement characteristics. Dislocation motion in crystalline materials, by movement in the plane along the dislocation line, is known as slip (glide). In order to allow these movements, all the bonds between the atoms must be broken [40]. This creep process is active in the whole temperature range and at high temperatures creep can occur below the yield stress, but the contribution is usually insignificant at low temperatures [41, 42].

Dislocation movement out of the dislocation plane by the means of vacancy-atom exchange, is known as dislocation climb. This occur when the dislocation movement is impeded by an obstacle (a point defect) and when vacancy diffusion is present. The dependence on vacancy diffusion makes this process more active during elevated temperatures [42, 43].

The process in which grains slide past each other along the boundaries is called grain-boundary sliding (GBS) and is caused by shear stresses acting on the these boundaries. Materials with small grains (large number of grains) act as barriers against sliding thus providing creep strength. Although, materials that have large grains (a low number of grain boundaries) does not contain as much vacancies and therefore dislocation climb are reduced compared to small-grained materials. Thus the grain size have dual effect on creep

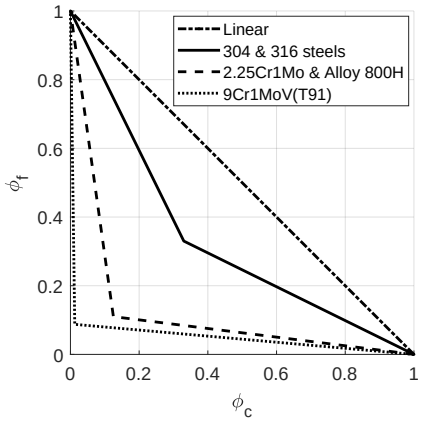

Figure 3: Example of a creep-fatigue damage envelope (interaction diagram) re-plotted from ASME Code [32] with axes interchanged (same as in [33]).

properties [41–43]. Voids and cavities is thought to be preceded by GBS, but it is unclear if the void formation is associated with or a consequence of GBS. As presented in the previous chapter, GBS can be prevented by precipitation in the grain boundaries [42].

Another creep mechanism is diffusion flow and it is caused by migration of vacancies through the lattice structure. This process requires the chemical bonds to be broken and reformed, thus a certain amount of activation energy is needed. At higher temperatures creep by diffusion flow is therefore more easy [41, 43].

The effect of creep damage on the fatigue endurance at elevated temperature is referred to as creep-fatigue interaction. The acceleration of fatigue damage due to the reduction of ductility caused by creep, is thought to be the main creep-fatigue damage mechanism [10]. However, with a more pessimistic analysis the account of the effects of fatigue upon creep are also considered [33].

ASME Code [32] uses creep-fatigue damage diagrams for proposed service cycles, where the creep and fatigue damage is evaluated separately. This is done by linear summation, using Miners rule for the fatigue damage (independent of strain rate) and time fraction summation to account for creep damage. The combined formulation can be seen in eq. 1.

$$\sum(n/N_d)_j + \sum(\triangle t/T_d)_k \leq D \tag{1}$$

In the above expression D is the allowable creep-fatigue damage factor, $(N_d)_j$ is the number of allowable cycles of type j, $(T_d)_k$ is allowable time at stress level k, n is actual number of cycles of type j and $\triangle$t is the actual time at stress level k [32, 33]. D is consequently the factor that account for the interacting effect of creep damage (due to time subjected to an applied stress) with generated fatigue cyclic damage. Values of D for steels from diffrent groups; one ferritic-martensitic (T91), three austenitic (304, 316, 800HT) and one bainitic (2.25Cr1Mo), at elevated temperatures ($\approx$ 425 °C) are shown in the creep-fatigue interaction diagram in Fig. 3. For 9CrMoV, the figure indicates high creep-fatigue interaction effect and that the allowable damage fraction for creep is very low in order to be in the safe design region. Although, Skeleton et al. [33] argues that this method of damage assessment can be somewhat pessimistic. Presented below are the types of creep-fatigue damage in austenitic alloys assessed by Plumbridge [44] and Hales [45].

- Transgranular crack initiation and growth
- Transgranular initiation followed by intergranular growth
- Intergranular initiation followed by transgranular growth
- Intergranular initiation and growth
- Internal triple point wedge crack
- Grain boundary voids
- Initiation from matrix pore or inclusion

In addition, the propagation can be "competing", "interacting" and "additive" according to [33, 45]. In "competing" propagation, each mechanism is independent of the other and follows its own failure criterion. In "additive" propagation, the mechanism act independently at the beginning but failure occurs when the combined damage reach unity. In "interacting" propagation, creep damage formation influences transgranular cracks so that the crack propagation is changed to intergranular characteristics. It is found that in such cases the total damage D becomes less than unity [33].

4

Experimental and analytical methods

In this chapter the experimental and analytical procedures are described. The investigated materials of the research project are presented first. Then the mechanical testing procedures are explained, followed by presentation of the different microstructural investigation methods used.

The TMF testing, hardness testing, creep-LCF testing, some creep tests and some ageing were conducted at Linköping University in Linköping. Long-term ageing and long-term creep tests were carried out at AB Sandvik Materials Technology in Sandviken, Sweden. The software Thermo-Calc together with the TCFE9 (Steels and Fe-Alloys) database were used for equilibrium simulations of the precipitation process for the investigated materials.

4.1 Material

This thesis involve investigations of three commercial austenitic alloys: Sanicro 25 (solution heat treated at 1220 °C for 10 minutes), Sanicro 31HT (solution heat treated at 1200 °C for 15 minutes) and Esshete 1250 (solution heat treated at 1100 °C for 15 minutes). Some specimens were also pre-aged, before TMF and CF testing, for 2000 hours at 650 °C, 700 °C and 800 °C.

These three alloys are meant to represent different types of austenitic alloy candidates for critical power plant boiler section components. Sanicro 25 are relative new and highly alloyed, Sanicro 31HT have increased nickel content and are also highly alloyed and Esshete 1250 are medium alloyed. The nominal chemical composition in wt.% of these materials are given in Table. 1. The materials were provided and heat-treated by Sandvik Materials Technology AB.

Table 1: Chemical composition (in wt.%) of the austenitic alloys (Fe=bal.).

Material	Cr/Ni	W/Co	Cu/Mn	Nb/N	Si/V	Mo/Ti	Al/C
Sanicro 25	22.5/25.0	3.6/1.5	3.0/0.5	0.5/0.23	0.2/-	-/-	-/0.1
Sanicro 31 HT	20.5/30.5	-/-	-/0.6	-/-	0.6/-	-/0.5	0.5/0.7
Esshete 1250	15/9.5	-/-	-/6.3	1.0/-	0.5/0.3	1.0/-	-/0.1

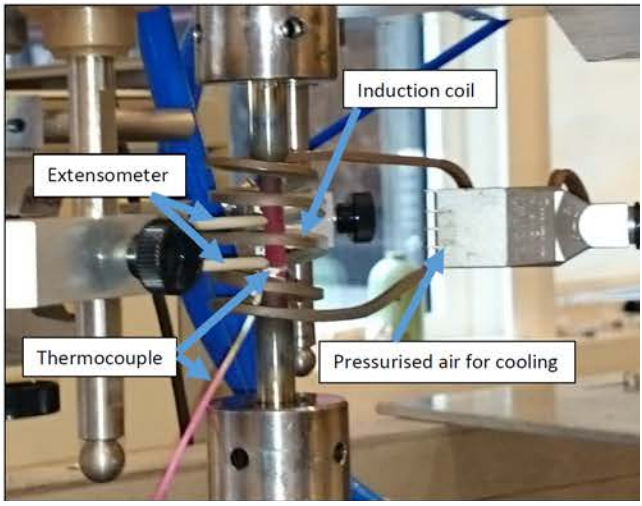

Figure 4: The setup for the TMF test machine.

4.2 Mechanical testing

In the following sections the mechanical testing are presented and in addition to these Vickers hardness testing was performed using Struers DuraScan G5, following ISO 6507 and ASTM E384 standards and with HV5 indenter configuration.

4.2.1 Thermomechanical fatigue testing

The used testing procedure was strain controlled thermomechanical fatigue (TMF) testing with 5 minutes dwell time at maximum mechanical strain ($\varepsilon_{\text{mech, max}}$) and maximum temperature. The test machine was a servo-hydraulic TMF machine from Instron with induction heating and forced air-cooling. The TMF test machine setup is shown in Fig. 4. Before the TMF tests the machine was carefully aligned, to prevent buckling and other

instability effects, according to "the validated code of practice" [9]. This study only includes the in-phase cycle with R_{ε}= 0. The temperature range used was 100 °C to 800 °C and the heating and cooling rate was 5 °C/s. The setup of the tests were done according to [9], with spot welded thermocouples in the middle of the gauge length at a distance of 1 mm between each other. The strain was measured with a high-temperature extensometer with a gauge length of 12.5 mm. The thermal strain was subtracted from the measured total strain, so that the mechanical strain could be controlled as suggested by [9]. The number of cycles to failure (N_f) was defined as the point at which the amplitude stress (σ_a) decrease 10 % below the tangent line constructed at the last point of zero curvature. Although, the test was not stopped until a load drop of 60 % occurred.

4.2.2 Creep-LCF testing

The mechanical testing were performed using an MTS servo hydraulic testing machine equipped with an Instron 8800 control system. The strain was measured by an Instron 2632-055 extensometer and the isothermal condition, at 700 °C, was controlled by an MTS 652.01 furnace. The R_{ϵ} = 0-type test cycle involved a strain controlled part, dashed line in Fig. 5, and a load controlled part, solid line in Fig. 5. Strain ranges from 0.5 % to 1.0 % and dwell times, t_d, from 0 to 1800 seconds were tested. Setup and employment of the test as well as definition of plastic strain range, $\triangle\epsilon_p$, stress range, $\triangle\sigma$, and total strain amplitude, $\triangle\epsilon/2$, were conducted according to ASTM standard E2714-3 for creep-fatigue testing [46]. The number of cycles until failure, N_f, was defined as the point at which the amplitude stress, $\triangle\sigma/2$, decrease 10% below the tangent line constructed at the last point of zero curvature, as suggested by [46].

4.3 Microscopy

4.3.1 Specimen preparation

The surface of the investigated samples must be carefully prepared in order reduce the surface roughness. This is important to be able to perform qualitative scanning electron microscopy (SEM) techniques like backscatter electron (BSE) and electron backscatter diffraction (EBSD). Mechanical polishing according to the steps in Table. 2 were performed on all the samples before the microscopic investigations.

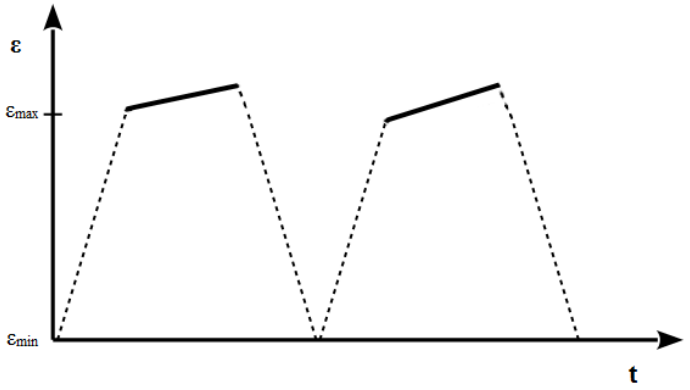

Figure 5: Sketch of the creep-LCF test cycle, strain vs. time

Table 2: Steps of the sample preparations.

Grinding paper/ polishing cloth	Grain size [μ]	Time [min]	No. papers
SiC paper, 500	30	4	2
SiC paper, 1200	15	4	1
SiC paper, 4000	5	4	3
Silk cloth	Diamond suspension, 3	8	
Woven wool cloth	Diamond suspension, 1	10	
Rayon-viscose fibres cloth	Diamond suspension, 0.25	15	
Neoprene foam cloth	Colloidal silica suspension, 0.04	5	
Neoprene foam cloth	water	1	

4.3.2 Scanning electron microscopy

Different SEM techniques like secondary electron (SE), backscattered electron (BSE), electron backscatter diffraction (EBSD) and energy dispersive spectroscopy (EDS) were used in the microstructural investigations of this project.

In investigations of the topographical information of cracks, the the SE-technique were used. Electrons emitted from the sample with very low energies (below 50eV) are considered secondary electrons (SE) and they originate from inelastic scattering on loosely bound outer shell electrons in the surface or the near surface regions of the samples (emission depth of $\approx$ 1nm). This gives a shallow escape depth and the surface contrast comes from the differ-

ence of number of electrons leaving the sample at different beam locations (number component) and contrast effects from the electron travel paths after leaving the sample (trajectory component) [47, 48].

In investigations that required compositional contrast imaging, the BSE-technique were used. The contrast comes from high energy (50 eV) backscattered electrons (BSE), that elastically returns from the sample and are collected by the BSE detector. Larger atoms, with greater atomic number (Z) have higher probability of producing an elastic collision because of their greater cross-sectional area. The number of BSE reaching the BSE detector is proportional to the mean atomic number of the sample. Thus, "brighter" BSE intensity correlates with greater average Z in the sample, and "dark" areas have lower average Z [47, 49]. This is used to distinguish between different phases and precipitates, but the technique can also provide topographic and crystallographic information.

The EDS technique was used for qualitative (element present) and quantitative (amount of elements) chemical analysis. This was done by measuring of the energy and intensity distribution of the x-ray photons signal that are generated from the focused electron beam and specimen interaction volume beneath the specimen surface. X-ray photons that emerge from the specimen have specific energies that relate to the elements in the sample. The relative weights of the characteristic X-ray lines in each family (different energies for different transitions between the subshells e.g. K, L, M of the specific atom) are consistent and this, along with their energies, allows related peaks in the X-ray spectrum to be recognized [47, 49]. The relative intensities of the elemental peaks was evaluated using a commercial software from Oxford. Information about the composition of phases and precipitates were collected with this technique.

The EBSD technique was used for obtaining information on the individual orientation of the microscopic grains. The EBSD pattern are gathered by illuminating a tilted specimen with the stationary electron beam. The diffraction/channelling of the electrons causes the electrons to form very flat cones. These cones have an angle of (90° - θ_b), where θ_b is the angle for Bragg reflection to occur. Because of diffraction from both back and front of the atomic planes, two pairs of cones intercept the imaging plane. These are viewed as two nearly straight lines separated by an angle of θ_b. The intersections of the different lines ("Kikuchi lines") represent zone axes and are related to a specific crystallographic direction within the crystal [47, 50, 51]. EBSD software use the Kikuchi pattern to identify the phase and the orientation of the crystal lattice in the point which generated the pattern, this process is referred to as indexing. During this process the actual Kikuchi pattern is compared to theoretical pattern and the mean angular deviation

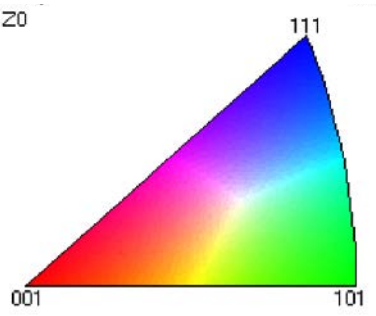

Figure 6: IPF colouring key legend.

(MAD value) between these two is considered a quality factor for the indexing process [47, 50]. Position of grain boundaries are defined with a minimum crystallographic orientation between neighbouring grid points (typically 10°). The orientation, shape and size of the grains can then be displayed using inverse pole figures (IPFs), which uses the stereographic triangle to express which crystal direction is parallel to the sample direction (surface normal, Z0) [50]. This is represented with colour code and for cubic materials the axis are red for [001], blue for [111] and green for [101], this is shown in Fig. 6.

The microscopic investigations using EBSD, EDS, SE, and BSE were performed in a HITACHI SU-70 FEG-SEM equipped with OXFORD EBSD and BSE detector. The EBSD system used the HKL software CHANNEL 5. The EBSD maps were measured with acceleration voltage of 20 kV using a working distance of 22 mm to 27 mm and step sizes of 0.5 μm to 1.5 μm. The SE and BSE images were captured using 10kV to 20 kV acceleration voltage and a working distance from 7.4 mm to 15 mm. The EDS process used 20 kV acceleration voltage and a working distance of 15 mm.

5

Summary and discussion of appended papers

Paper I

Creep-fatigue interaction in heat resistant austenitic alloys

In this paper the combined effect of creep and fatigue was investigated for the two austenitic stainless steels Sanicro 25 and Esshete 1250. The mechanical tests were conducted by strain controlled low-cycle fatigue, with load controlled dwell times. The tests had variable strain amplitudes and dwell times, and the test temperature was 700 °C. From, the test data hardening/softening curves (stress vs. cycles/time), hysteresis curves (stress vs. strain) and a creep-fatigue interaction diagram, were constructed and analysed. With the data analyses and previous work from the literature, estimated damage initiation mechanisms were discussed. It was found that both the investigated materials suffered from interaction damage by creep and fatigue for most of the test configurations. Different type of estimated initiation and propagation damage were active depending on the duration of the dwell time and the amplitude of the strain. Of the two investigated materials, Sanicro 25 suffered higher stresses and showed longer creep-fatigue cycle life.

Paper II

Fracture and Damage Behaviour in an Advanced Heat Resistant Austenitic Stainless Steel During LCF, TMF and CF

This paper summarises and discuss fracture and damaging behaviours of Sanirco 25 exposed to various testing conditions. These involve two types of IP TMF tests, creep-fatigue tests and LCF tests. The cyclic behaviour for the different testing conditions were analysed and compared. The results revealed that Sanicro 25, in TMF and CF conditions, clearly suffered shorter fatigue cycle life compared to LCF conditions. It was also indicated from the mechanical test data that the TMF and CF conditions were influenced differently by pre-ageing. Pre-ageing had a positive impact on the CF-life and a negative impact on the TMF-life. However, the ageing temperatures were lower in the CF case and too few tests were performed. Thus a final conclusion could not be establish. During the TMF testing condition, Sanicro 25 showed prominent cyclic hardening and this effect was further promoted by higher strain ranges, lower dwell times, lower temperature ranges and pre-ageing.

The microscopic investigations of the fracture and damage behaviour showed evidence of oxidation assisted cracking in TMF tested specimens and damage by void formation in CF tested specimens. For TMF and CF conditions, EBSD mapping showed crack initiation in multiple grain boundaries at the surface.

Paper III

Thermomechanical Fatigue Behaviour of Aged Heat Resistant Austenitic Alloys

This paper focuses on the influence of pre-ageing on the TMF behaviour for the three austenitic stainless steels Sanicro 25, Esshete 1250 and Sanicro 31HT. The aim was to investigate the influence of prolonged service degradation, simulated by pre-ageing at 800 °C for 2000 hours. The TMF tests were performed with IP loading, temperature ranges of 100 °C to 800 °C and dwell times of 5 minutes at maximum temperature. The role of precipitation and damaging mechanisms were investigated using the SEM techniques BSE, EDS and EBSD.

The investigation showed that all the tested materials experienced detrimental effects from pre-ageing and this were considered to be because of

the deterioration by the microstructural evolution, which foremost enabled oxidation assisted cracking and reduced the creep resistance.

Discussion

This thesis has the overall aim to give a better understanding of the influence of detrimental high-temperature cyclic conditions on the candidates for critical components in boiler sections of next generation power plants. In Chapter 1.4 the overall aim was formulated as three research questions, RQ1, RQ2, and RQ3. RQ1 and RQ2 are answered by the summery of appended papers above. Where the response, behaviour and influence of pre-ageing of the investigated materials subjected to CF conditions (paper 1 and 2) and TMF conditions (paper 2 and 3) are presented.

To be able to answer RQ3, an overall assessment of the research performed within this thesis must be considered. In CF conditions, both Esshete 1250 and Sanicro 25 showed interaction damage. Although Sanicro 25 suffered higher stresses, the alloy showed longer CF-life compared to Esshete 1250. This should relate to higher creep resistance at higher stresses, which is also shown in the TMF investigations of paper 3 where Sanicro 25 have the longest TMF-life, both for the virgin and pre-aged condition. In compliance with the theory in chapter 3.1, creep is the dominant damaging mechanism during IP TMF, which should indicate that the material with best creep resistance also has the longest TMF-life. Compared to the other investigated materials, Essehete 1250 had the biggest negative impact from pre-ageing and it was found that the microstructure was highly deformed even at lower mechanical strain ranges. As discussed in paper 3, the microstructural evolution is important for the high temperature strength and for Esshete 1250 strengthening mechanisms (mainly coarsening of NbC precipitates), resistance to creep (depletion of Mo) and resistance to oxidation (depletion of Cr and Mo along with low amount of Cr in the alloy) were found to deteriorate at these conditions. The same detrimental effects are also found for the other two alloys however, they show better resistance to these effects. In particular, during these conditions, Sanicro 25 has more effective strengthening mechanisms like finely dispersed MX precipitates and Z-phases. These mechanisms were not found in Sanicro 31HT, instead excessive precipitation of carbides ($M_{23}C_6$) were found to embrittle the grain boundaries. This process was also found in Sanicro 25 but not i the same order of magnitude, due to the formation of other carbon containing phases and precipitates.

This reasoning give an explanation to why Sanicro 25 showed superior TMF and CF response, even though the damaging process at these conditions

were found to be complicated.

6

Conclusions and future work

The presented research within this licentiate thesis deals with high-temperature behaviour of austenitic alloys with focus on the damaging mechanisms during thermomechanical fatigue (TMF) and creep-fatigue (CF) interaction conditions. In addition, the influence of prolonged service degradation was evaluated for the investigated materials by pre-ageing.

It was found that both Sanicro 25 and Esshete 1250 suffered from creep-fatigue interaction damage and it was concluded that different type of estimated initiation and propagation damage were active depending on the duration of dwell time and the amplitude of strain. Sanicro 25 suffered higher maximum stresses but still showed superior creep-fatigue cycle life compared to Esshete 1250 during CF at high temperatures.

TMF and CF loading conditions, proved to be more detrimental for Sanicro 25 than isothermal LCF conditions. Sanicro 25 showed prominent cyclic hardening and this effect is further promoted by increased strain ranges, decreased dwell times, decreased temperature ranges and pre-ageing. For LCF, TMF and CF conditions crack initiation appeared in multiple grain boundaries at the surface of the specimen. The crack initiation in the three different test conditions were oxidation assisted and damage by void formation were also found in the CF tested specimens.

All the investigated materials experienced a detrimental effect from pre-ageing, this was due to the negative microstructural evolution during high temperature TMF cycling. Creep and oxidation assisted cracking were considered the most damaging mechanism in the TMF process.

Compared with the other investigated materials, Sanicro 25 was found to be the best candidate suited for critical components in the boiler sections of the next generation power plants. This is motivated by the more effective microstructural evolution and strengthening mechanisms, which promotes

higher resistance to damage originating from creep, creep-fatigue interaction and oxidation.

Given these conclusions, the next step for future work which are in line with this research will now be discussed.

In order to further investigate the use of austenitic stainless steels as candidates for next generation power plants, comparisons to reference materials that are commonly used in power plants, such as different ferritic stainless steels, would be of interest. In order to receive a broader picture of the damaging behaviours of the materials during these conditions, investigations including other important high temperature properties like fatigue crack propagation resistance, toughness and structure stability/integrity could be beneficial. In this context the investigations could also include the behaviour of welded components, which are common in power plants. The influence of ageing should be investigated further including longer ageing times and variable temperatures, given the indication of enhanced CF-life for Sanirco 25. Also, more work still remains on the investigation of the microstructural evolution during high temperature CF conditions. Further TMF investigations including various temperature ranges and OP loading condition would be of interest to gain more knowledge of the material behaviour for additional high temperature conditions. Future investigations could also include interrupted testing in order to assess the progression of the occurring detrimental effects.

Bibliography

[1] World Energy Council. Renewable Energy Projects Handbook. Technical Report April, World Energy Council, London, 2004. URL https://www.worldenergy.org/wpcontent/uploads/2012/10/PUB_Renewable_Energy_Projects_Handbook_2004_WEC.pdf.

[2] World Energy Council. World Energy Resources 2013, 2013. URL https://www.worldenergy.org/publications/2013/worldenergy-resources2013survey/.

[3] Ayhan Demirbas. Potential applications of renewable energy sources, biomass combustion problems in boiler power systems and combustion related environmental issues. *Prog. Energy Combust. Sci.*, 31(2):171-192, 2005. ISSN 03601285. doi: 10.1016/j.pecs.2005.02.002.

[4] Kristin Dietrich, Jesus M. Latorre, Luis Olmos, and Andres Ramos. The Role of Flexible Demands in Smart Energy Systems. In *Energy Syst.*, chapter Optimizati, pages 79-97. Springer, 2013. ISBN 9783642381331. doi: 10.1007/9783642381348_4.

[5] Eurelectric. Flexible generation: Backing up renewables, 2011. URL https://www.gasnaturally.eu/uploads/Modules/Publications/flexibility_report_final201110200030e[1]2.pdf.

[6] Jiamin YIN and Zhansong WU. Corrosion Behavior of TP316L of Superheater in Biomass Boiler with Simulated Atmosphere and Deposit. *Chinese J. Chem. Eng.*, 17(5):849-853, 2009. ISSN 10049541. doi: 10.1016/S10049541(08)602864.

[7] R. Viswanathan, K. Coleman, and U. Rao. Materials for ultra-supercritical coalfired power plant boilers. *Int. J. Press. Vessel. Pip.*, 83(1112):778-783, nov 2006. ISSN 03080161. doi: 10.1016/j.ijpvp.2006.08.006.

[8] Hans-Jürgen Christ. Effect of environment on thermomechanical fatigue life. *Mater. Sci. Eng. A*, 468470:98-108, nov 2007. ISSN 09215093. doi: 10.1016/j.msea.2006.08.132.

[9] Peter Hähner, Ernst Affeldt, Tilmann Beck, Hellmuth Klingelhöffer, Malcolm Loveday, and Claudia Rinaldi. Final version of the Validated Code-of-Practice for Thermo-Mechanical Fatigue Testing. Technical Report June, European Comission: Directorate-General Joint Research Centre (DG JRC) and Institute for energy, Petten (Netherlands), 2006.

[10] Yukio Takahashi. CreepFatigue Interaction Its Mechanism and Predictability. In *Asian Pacific Conf. Mater. Mech. 2009*, pages 1-4, 2009.

[11] International Stainless Steel Forum. Stainless Steel in Biogas Production A Sustianable Solution for Green Energy, 2012. URL `www.worldstianless.org`.

[12] L C Casteletti, A L Neto, and G E Totten. Nitriding of Stainless Steels. In *ASM Handb.*, chapter Heat Treating of Iron and steel, pages 418-438. ASM International, vol 4d edition, 2014. ISBN 9781627080668.

[13] Barbara Rossi. Discussion on the use of stainless steel in constructions in view of sustainability. *ThinWalled Struct.*, 83:182-189, oct 2014. ISSN 02638231. doi: 10.1016/j.tws.2014.01.021.

[14] K. H. Lo, C. H. Shek, and J. K.L. Lai. Recent developments in stainless steels. *Mater. Sci. Eng. R Reports*, 65(46):39-104, 2009. ISSN 0927796X. doi: 10.1016/j.mser.2009.03.001.

[15] Harry Bhadeshia and Robert Honeycombe. Chapter 12 : Stainless Steel. In *Steels Microstruct. Prop.*, chapter 12, page 488. Butterworth-Heinemann, 4 edition, 2017. ISBN 9780081002704.

[16] A. Di Gianfrancesco, editor. *Materials for UltraSupercritical and Advanced UltraSupercritical Power Plants*. Elsevier, 2017. ISBN 9780081005521. doi: 10.1016/C20140048265.

[17] T. Sourmail. Precipitation in creep resistant austenitic stainless steels. *Mater. Sci. Technol.*, 17(1):1-14, jan 2001. ISSN 02670836. doi: 10.1179/026708301101508972.

[18] ASM international. Physical Metallurgy of Stainless Steels. In *ASM Handb.*, chapter Medical Ap, pages 199-210. ASM international, vol 23 edition, 2012.

[19] M. Heczko, B. D. Esser, T. M. Smith, P. Beran, V. Mazánová, D. W. McComb, T. Kruml, J. Polák, and M. J. Mills. Atomic resolution characterization of strengthening nanoparticles in a new high-temperaturecapable 43Fe25Ni22.5Cr austenitic stainless steel. *Mater. Sci. Eng. A*, 719(December 2017):49-60, 2018. ISSN 09215093. doi: 10.1016/j.msea.2018.02.004.

[20] Vlastimil Vodárek. Creep behaviour and microstructural evolution in AISI 316LN+Nb steels at 650°C. *Mater. Sci. Eng. A*, 528:4232-4238, 2011.

[21] G F Vander Voort, G M Lucas, and E P Manilova. Metallography and Microstructures of Stainless Steels and Maraging Steels. In G F Vander Voort, editor, *ASM Handb.*, pages 670-700. ASM international, vol 9 edition, 2014.

[22] Grzegorz Golański, Adam Zieliński, and Hanna Purzyńska. Precipitation Processes in CreepResistant Austenitic Steels. In *Austenitic Stainl. Steels - New Asp.* InTech, dec 2017. doi: 10.5772/intechopen.70941.

[23] T. Sourmail and H. K. D. H. Bhadeshia. Microstructural evolution in two variants of NF709 at 1023 and 1073 K. *Metall. Mater. Trans. A*, 36 (1):23-34, jan 2005. ISSN 10735623. doi: 10.1007/s11661005-0135y.

[24] Dae-Bum Park, Sung-Min Hong, Kyu-Ho Lee, Moo-Young Huh, Jin-Yoo Suh, Seung-Cheol Lee, and Woo-Sang Jung. Hightemperature creep behavior and microstructural evolution of an 18Cr9Ni3CuNbVN austenitic stainless steel. *Mater. Charact.*, 93:52-61, jul 2014. ISSN 10445803. doi: 10.1016/j.matchar.2014.03.012.

[25] Chih-Chun Hsieh and Weite Wu. Overview of Intermetallic Sigma (σ-phase) Phase Precipitation in Stainless Steels. *ISRN Metall.*, 2012(4): 1-16, 2012. ISSN 20908717. doi: 10.5402/2012/732471.

[26] Ying Yang, Lizhen Tan, and Jeremy T. Busby. Thermal Stability of Intermetallic Phases in Ferich FeCrNiMo Alloys. *Metall. Mater. Trans. A*, 46(9):3900-3908, sep 2015. ISSN 10735623. doi: 10.1007/s11661015-2997y.

[27] Yasushi Kato, Masatoshi Ito, Yoshimine Kato, and Osamu Furukimi. Effect of Si on Precipitation Behavior of Nb-Laves Phase and Amount of Nb in Solid Solution at Elevated Temperature in High Purity 17%Cr-0.5%Nb Steels. *Mater. Trans.*, 51(9):1531-1535, 2010. ISSN 13475320. doi: 10.2320/matertrans.M2010112.

[28] Imanuel Tarigan, Naoki Takata, and Masao Takeyama. Grain Boundary Precipitation Strengthening Mechanism by Fe 2 Nb Laves Phase in Creep of Fe20Cr30Ni2Nb Austenitic Heat Resistant Steel. *Creep Fract. Eng. Mater. Struct. Japan Inst. Met.*, 2012.

[29] J Okrajni. Thermomechanical fatigue conditions of power plant components. *J. Achiev. Mater. Manuf. Eng.*, 33(1):53-61, 2009.

[30] R Viswanathan and J. Stringer. Failure Mechanisms of High Temperature Components in Power Plants. *J. Eng. Mater. Technol.*, 122(3): 246-255, 2000. ISSN 00944289. doi: 10.1115/1.482794.

[31] Yasutaka Noguchi, Hirokazu Okada, Hiroyuki Semba, and Mitsuru Yoshizawa. Isothermal, thermo-mechanical and bithermal fatigue life of Ni base alloy HR6W for piping in 700°C USC power plants. *Procedia Eng.*, 10:1127-1132, 2011. ISSN 18777058. doi: 10.1016/j.proeng.2011.04.186.

[32] Robert Jetter. Subsection NH Class 1 Components in Elevated Temperature Service. In *Companion Guid. to ASME Boil. Press. Vessel Code, Vol. 1, Third Ed.*, chapter 12, pages 409-445. ASME, Three Park Avenue New York, NY 10016-5990, 2007. doi: 10.1115/1.802694.ch12.

[33] R.P. Skelton and D. Gandy. Creep fatigue damage accumulation and interaction diagram based on metallographic interpretation of mechanisms. *Mater. High Temp.*, 25(1):27-54, mar 2008. ISSN 09603409. doi: 10.3184/096034007X300494.

[34] L.R Li, W Chen, J.G Sheng, X.P Wu, and H.F Mao. Creepfatigue life design and calculation method for boiler pressure elements under elevated temperature. *Dongli Gongcheng/Power Eng.*, 5:409-416, 2009.

[35] A Nitta and K Kuwabara. ThermalMechanical Fatigue Failure and Life Prediction. *Curr. Japanese Mater. Res.*, 3:203-222, 1988.

[36] Keun Ho Bae, Hyun Ho Kim, and Soon Bok Lee. Competing damage mechanisms in the thermomechanical fatigue of AISI 304L stainless steel. *Mater. Sci. Eng. A*, 529(1):417-424, 2011. ISSN 09215093. doi: 10.1016/j.msea.2011.09.054.

[37] Mageshwaran Ramesh, Hans J. Leber, Koenraad G.F. Janssens, Markus Diener, and Ralph Spolenak. Thermomechanical and isothermal fatigue behavior of 347 and 316L austenitic stainless tube and pipe

steels. *Int. J. Fatigue*, 33(5):683-691, 2011. ISSN 01421123. doi: 10.1016/j.ijfatigue.2010.11.005.

[38] A. Nagesha, M. Valsan, R. Kannan, K. Bhanu Sankara Rao, V. Bauer, H. J. Christ, and Vakil Singh. Thermomechanical fatigue evaluation and life prediction of 316L(N) stainless steel. *Int. J. Fatigue*, 31(4):636-643, 2009. ISSN 01421123. doi: 10.1016/j.ijfatigue.2008.03.019.

[39] R. Petráš, V. Škorík, and J. Polák. Thermomechanical fatigue and damage mechanisms in Sanicro 25 steel. *Mater. Sci. Eng. A*, 650:52-62, jan 2016. ISSN 09215093. doi: 10.1016/j.msea.2015.10.030.

[40] V. Gerold and H.P. Karnthaler. On the origin of planar slip in f.c.c. alloys. *Acta Metall.*, 37(8):2177-2183, aug 1989. ISSN 00016160. doi: $10.1016/0001 - 6160(89)90143 - 0$.

[41] Richard W Hertzberg, Richard P Vinci, and Jason L Hertzberg. *Deformation and Fracture Mechanics of Engineering Materials*. Wiley, John Wiley and Sons INC, fifth edition, 2013. ISBN 9780470527801.

[42] Joshua Pelleg. General Mechanisms of Creep. In *Solid Mech. its Appl.*, volume 241, pages 41-61. Springer, 2017. ISBN 9783319508252. doi: 10.1007/9783319508269_4.

[43] J.C Gibeling. Creep Deformation of Metals, Polymers, Ceramics, and Composites. In *ASM Handb. online*, chapter vol 8, pages 363-368. ASM international, 2000.

[44] W.J. Plumbridge. Uprating and life assessment under fatiguecreep conditions. *Int. J. Press. Vessel. Pip.*, 59(13):119-129, jan 1994. ISSN 03080161. doi: 10.1016/03080161(94)901473.

[45] Royden Hales. A Quantitative Metallographic Assessment of Structural Degradation of Type 316 Stainless Steel During Creep Fatigue. *Fatigue Fract. Eng. Mater. Struct.*, 3(4):339-356, oct 1980. ISSN 8756758X. doi: 10.1111/j.14602695.1980.tb01383.x.

[46] ASTM. Creep Fatigue Testing, 2014. URL `www.astm.se`.

[47] Joseph I. Goldstein, Dale E. Newbury, Joseph R. Michael, Nicholas W.M. Ritchie, John Henry J. Scott, and David C. Joy. *Scanning Electron Microscopy and XRay Microanalysis*. Springer New York, New York, NY, 2018. ISBN 9781493966745. doi: 10.1007/9781493966769.

[48] M T Postek, K S Howard, A H Johnson, and K L McMichael. *Scanning Electon Microscopy A student's Handbook*. Ladd Research Industries Inc, 1980.

[49] H E Exner and S Weinbruch. Scanning Electron Microscopy. In *ASM Handb.*, chapter Metallogra, pages 355-367. ASM international, vol 9 edition, 2004.

[50] Adam J. Schwartz, Mukul Kumar, Brent L. Adams, and David P. Field, editors. *Electron Backscatter Diffraction in Materials Science*. Springer US, Boston, MA, 2009. ISBN 9780387881355. doi: 10.1007/9780387-881362.

[51] Valerie Randle. Electron backscatter diffraction : Strategies for reliable data acquisition and processing. *Mater. Charact.*, 60(9):913-922, 2009. ISSN 10445803. doi: 10.1016/j.matchar.2009.05.011.

Papers

The papers associated with this thesis have been removed for copyright reasons. For more details about these see:

http://urn.kb.se/resolve?urn=urn:nbn:se:liu:diva-153100